# Use of Integrated Photovoltaic-Electric Spring System as a Power Balancer in Power Distribution Networks

Tianbo Yang, *Student Member, IEEE*, Kwan-Tat Mok, *Student Member, IEEE*, Siu-Shing Ho, Siew-Chong Tan, *Senior Member, IEEE*, Chi-Kwan Lee, *Senior Member, IEEE*, and Ron S. Y. Hui, *Fellow, IEEE*

***Abstract*—Electric springs (ES) have been proposed as a demand-response technology for improving the stability and power quality of emerging power systems with high penetration of intermittent renewable energy sources. Existing ES applications mainly involve the regulations of grid voltage and utility frequency. This paper reports a power control and balancing technique for a new integrated configuration of ES and photovoltaic (PV) system, and discusses its possible use to achieve dynamic supply–demand balance in power distribution networks. The proposed system enables delivery of maximally harvested PV power to the grid via the ES, and concurrently controls the active power consumption of its ES-associated smart load so as to achieve supply–demand power balance of the overall system in real time. Importantly, battery storage is not necessary in the proposed design because the ES-associated smart-load power follows an appropriate consumption profile to compensate potential prediction errors of the PV power generation. Both simulation and experimental results are included to validate the proposed ES system.**

***Index Terms*—Demand-side management, electric springs (ES), photovoltaic (PV) power generations, power imbalance.**

## I. Introduction

WITH increasing awareness on global warming issues and energy crisis, different forms of distributed energy resources (DER) such as photovoltaic (PV) power generations [1], [2], micro wind turbines [3], [4], electrical vehicles (EV) [5], [6], and fuel cells [7], [8], have been deployed into power grids over the last decades. With the advantages of a rapidly reduced cost and no rotational parts [9], [10], PV power generation systems have become an important distributed generation (DG) in

Manuscript received February 2, 2018; revised April 26, 2018 and July 23, 2018; accepted August 17, 2018. Date of publication August 28, 2018; date of current version April 20, 2019. This work was supported in part by the Hong Kong Research Grant Council under the theme-based project T23-701/14-N. Recommended for publication by Associate Editor K. A. Kim. *(Corresponding author: Siew-Chong Tan.)*

T. Yang, K.-T. Mok, S.-S. Ho, S.-C. Tan, and C.-K. Lee are with the Department of Electrical and Electronic Engineering, University of Hong Kong, Hong Kong (e-mail:

coordinated with other technologies in the power distribution networks with substantial PV power generations.

2) Reactive power compensation implemented on the PV inverters is a common method to alleviate the voltage rise issue in distribution networks [21]. For instance, the adaptive adjustment of the amount of reactive power injected from PV inverters is proposed in [22]. The limitation of this approach is that although the over-voltage problem can be mitigated, the real power imbalance between the supply and demand side cannot be handled.
3) Limiting the harvested PV active power is more effective than the reactive power control when regulating the grid voltage in power distribution networks [23]. The real power capping method has been proposed in view of preventing overvoltage by adaptively setting the power caps for PV power generation systems in real time [24]. A remote power controller is required to be installed in PV units for the curtailment of harvested PV power in accordance with the control signal received from the DNO [14]. The major drawback of this approach is that the energy harvesting capacity of the PV system is not fully utilized.
4) To maximize the amount of PV power generation, the integration of BESS overcomes the shortcoming of the PV active power capping approach. Also, BESS can be used for grid voltage regulation [25], [26], peak load shaving [12], and compensation of the fluctuating PV power [27]. However, this approach involves a massive deployment of batteries that induces environmental concerns [28]. Also, the high cost of batteries is another concern [29].
5) The demand-side management (DSM) has been found as a popular approach for solving various issues in emerging smart grids. The dynamic electricity pricing scheme, such as a time of use (TOU) pricing scheme [30] or an autonomous energy consumption scheduler [31], is a common method to realize the DSM. Studies based on such approaches have validated that DSM can play a role in reducing peak demand and mitigating supply–demand imbalance under normal conditions [30]–[32]. But pricing scheme is not an effective DSM method at extreme conditions. The recent power blackout in South Australia (when the temperature rose above 40 °C) is an example because consumers continued to turn ON their air-conditioners even if the electricity price was high [33].

This paper provides a DSM application based on electric springs (ES) to enhance the supply–demand power balance in a power distribution network. The original use of ES mainly focuses on grid voltage and frequency stabilization [34]–[36]. In the subsequent research works, the use of ES, via different circuit structures, has been extended to achieve more sophisticated functionalities. There are three primary types of ES proposed, namely the original ES (ES-1), the ES with battery (ES-2) [37], and the back-to-back ES (ES-B2B) [38]. Connected to a noncritical (NC) load in series, ES-1 can provide reactive power compensation directly and manipulate the active power consumption of the NC load indirectly. ES-2, which is built upon ES-1 but comprises battery storage, is able to provide bidirectional active power flow and thereby greatly broadens the operating range of ES. ES-B2B concurrently adopts a shunt (coupling with the grid) and a series ES (connecting the grid and the NC load). In such a way, the ES-B2B not only saves the cost of battery storage in ES-2, but also further expands the operating range of ES.

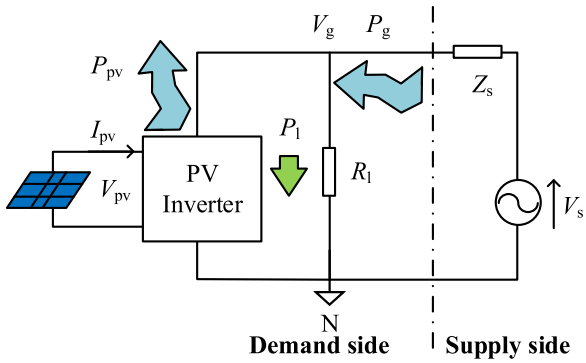


Fig. 1. Simple power grid with a conventional PV system installed. (The zigzag arrows indicate the uncertain power generations while the normal arrow indicates a stable power consumption.)

The new proposal in this paper integrates a distributed PV power system into an ES and its associated NC load to form a combined PV-ES system. Same as the original ES, the proposed PV-ES system still performs the DSM by essentially adjusting the voltage of the NC load. But different from all of the mentioned ES systems, this PV-ES system forms a new configuration in which the PV power is maximally harvested and the active power consumption of the system is precisely controlled by a new power flow control method. The PV-ES system can be used for compensating the integrated PV power with intermittency and balancing supply–demand power at the same time.

The main contributions of this paper are listed as follows:

1) An automatic and real-time DSM device integrating a PV system into an ES with an NC load to form a PV-ES system is proposed.
2) An ES-associated smart load is constructed within this PV-ES system. The active power consumption of this smart load can be adaptively adjusted in order to reduce supply–demand power imbalance.
3) A power-flow analysis and control scheme for this PV-ES system are included. The control method can precisely deliver the harvested PV power to the grid while accurately vary the active power consumption of the PV-ES system. In this way, a new solution against the intermittency of PV power is provided.
4) Battery storage is an option but not a necessity in the proposed PV-ES system. In this paper, the control method of the PV-ES system is evaluated without involving the usage of battery storage. Hence the costly batteries and the environmental concerns are avoided.

## II. Power Flow Control on PV-ES System

A schematic of a PV system connected to the point of common coupling (PCC) is shown in Fig. 1. The power grid is represented as a power source $V_s$ including a distribution line

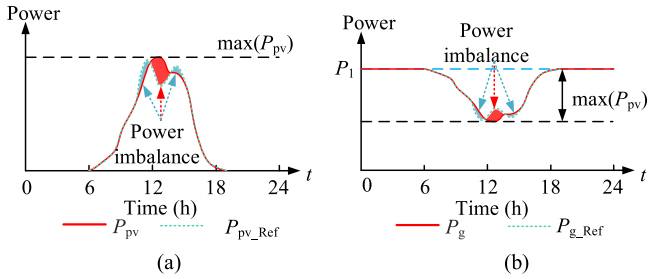


Fig. 2. Deviation between predicted and actual power generation/consumption. (a) PV power. (b) Demand-side power.

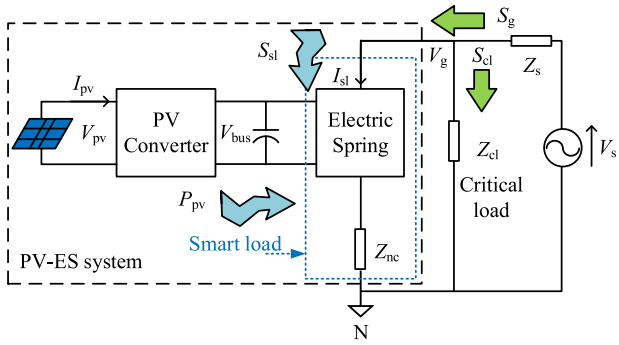


Fig. 3. Simplified diagram of the PV-ES system.

$Z_s$ on the supply side. A load $R_1$ and a PV system as shown in Fig. 1 are considered on the demand side. $V_g$ denotes the voltage RMS magnitude of PCC. The PV system is made up of a PV panel array, and an interfacing power inverter that converts and transfers the harvested renewable power $(P_{pv})$ to the power grid. The load $R_1$, consuming a real power $P_1$, represents the power consumption on the demand side.

The PV power generation at the demand side is predicted as $P_{\text{pv\_Ref}}$, and hence an expected supply-side power reference is estimated $(P_{\text{g\_Ref}} = P_1 - P_{\text{pv\_Ref}})$. Due to the uncertainty of the PV power generation, the PV power prediction is a great concern for the operators of the energy management in electricity networks with high integration of PV power. Accurate forecasting based on real-time measurements and records is helpful for operators to reduce the impact of the variability of PV power on the grid, and to improve the grid reliability [39]. However, such kinds of forecasting are easily influenced by the external conditions (such as the weather, temperature, and presence of dust). Therefore, the intermittent nature of PV generation still leaves inevitable errors between the predicted power $(P_{\text{pv\_Ref}})$ and actual power $(P_{pv})$. Since the supply-side reference is based on the forecasting, such errors cause the power imbalance between the supply and demand sides. Fig. 2(a) shows a sketch of the deviation between the predicted PV power and the actual harvested PV power in a period of 24 h (the deviation in practice will be more frequent and typically more severe). For the simplicity of the analysis, consider that the power $(P_1)$ consumed by the load $R_1$ is constant, the predicted $(P_{\text{g\_Ref}})$ and the actual $(P_g)$ power consumption on the demand side are plotted in Fig. 2(b), which corresponds to the PV power, as shown in Fig. 2(a). The shaded areas depicted in Fig. 2(a) and (b) illustrate the power imbalances of the harvested PV power and the demand-side power due to the errors, respectively. Both the over-power and under-power estimation can lead to supply–demand power imbalance, which could cause further power stability issues.

As a supply–demand power balancer, the proposed PV-ES system, as shown in Fig. 3, consists of a PV panel array, a PV converter, an ES, and an NC load. In the usual PV harvesting process, the dc power output of the PV converter forms the dc voltage for the ES. The equivalent impedance of the NC load is denoted as $Z_{nc}$. The remaining loads (not including $Z_{nc}$) in this power grid can be combined into a single critical load denoted as $Z_{cl}$. In this paper, we assume a heating or cooling system, which is purely resistive, as the NC load. With the characteristics of

1) being readily available throughout the 24-h timeframe,
2) having a great storage inertia in for buffering voltage fluctuation, and
3) being a widespread appliance commonly available in most of the buildings, such thermal loads are ideal NC candidates for ES applications.

The complex power consumed by the ES, the NC load, the critical load, and the ES-associated smart load are, respectively, denoted as $S_{es} = P_{es} + jQ_{es}, S_{nc} = P_{nc} + jQ_{nc}, S_{cl} = P_{cl} + jQ_{cl}$, and $S_{sl} = P_{sl} + jQ_{sl}$ (all symbols stand for magnitudes). For the ease of explanation in the subsequent analysis, the critical load is also chosen to be purely resistive $(Q_{nc} = Q_{cl} = 0)$.

There are two main objectives of using such PV-ES configuration. First, the ES should regulate the demand-side active power to be a desired value (a value determined by the upper level to maintain a constant power consumption for power balance, or to adjust the power consumption to participate in voltage/frequency regulation, etc.) irrespective of the fluctuation of the PV power generation. Second, the PV system and the ES should collaborate properly in such a way that the system can transfer the intermittent PV power to the grid without the need of battery storage. To handle the desired PV power delivery and to adaptively regulate the power consumption of the smart load simultaneously, two power references, 1) the ES active power reference $(P_{\text{es\_Ref}})$ and 2) the ES-associated smart-load active power reference $(P_{\text{sl\_Ref}})$ are required in the proposed control strategy. Based on the assumption that the power loss of the power converters is ignored in the analysis, and the fact that the PV converter is linked to the ES converter, as shown in Fig. 3, the amount of the harvested PV power $(P_{pv})$ should be equal to that of the ES active power delivered to the power grid $(-P_{es})$.[1]

In the proposed control scheme, the power consumption of the ES-associated smart load should be adjustable irrespective of the PV power fluctuation. The operation point of the ES with a given value of $P_{sl}$ can be derived based on the

[1]According to the $S_{\text{es}}$ defined, the negative polarity of the ES active power indicates that the active power is transferred from the ES to the power grid, and vice versa.

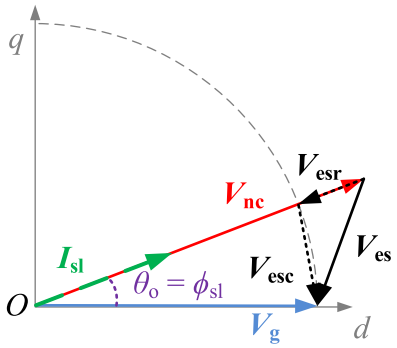


Fig. 4. Arbitrary diagram of the smart load voltage and current phasors.

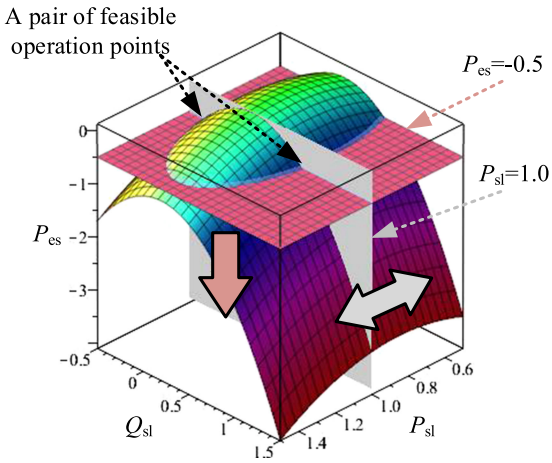


Fig. 5. Arbitrary normalized sketch of the circular paraboloid function.

radial-chordal decomposition (RCD) method [40]. To illustrate how the regulation can be achieved, an arbitrary phasor diagram of the smart load is shown in Fig. 4, where $V_{es}, V_{esr}, V_{esc}$, and $I_{sl}$, respectively, stand for the RMS magnitudes of the ES voltage, the radial component of the ES voltage (always in parallel with $V_{\text{nc}}$), the chordal component of the ES voltage, and the smart-load current (the same as the NC-load current). $\theta_o$ is the deviation between power factor angles of the smart load $(\phi_{sl})$ and the NC load $(\phi_{nc})$. As the NC load is purely resistive, $(\phi_{nc} = 0)$, $\theta_{\text{o}}$ is equal to the power angle of the smart load in this analysis. According to the circuit configuration shown in Fig. 3, the smart-load active power can be expressed as

$$P_{sl} = V_g \frac{(V_g - V_{esr})}{Z_{nc}} \cos\phi_{sl} = P_{es} + \frac{(V_g - V_{esr})^2}{Z_{nc}} \cos\phi_{nc} \tag{1}$$

and the apparent power of the smart load can be described as

$$S_{sl} = \sqrt{{P_{sl}}^2 + {Q_{sl}}^2} = V_g \left[\frac{(V_g - V_{esr})}{Z_{nc}}\right]. \tag{2}$$

Rearranging (1) and (2) leads to

$$P_{es} = -\frac{Z_{nc}\cos\phi_{nc}}{{V_g}^2}{P_{sl}}^2 - \frac{Z_{nc}\cos\phi_{nc}}{{V_g}^2}{Q_{sl}}^2 + P_{sl} \tag{3}$$

where $P_{es}$ is a paraboloid function of $P_{sl}$ and $Q_{sl}$ in a three-dimensional $P_{sl} - Q_{sl} - P_{es}$ space. Fig. 5 shows a plot of an arbitrary normalized paraboloid function of (3) for illustration.

With regard to (3), a given ES active power $(P_{es})$ corresponds to a set of defined combinations of the ES-associated smart-load active and reactive power ($P_{sl}$ and $Q_{sl}$). This set of combinations formulates an operating locus of $P_{sl}$ and $Q_{sl}$. This operating locus can be visualized, for example, by considering the interception points between the plane $P_{es} = -0.5$ p.u. and the paraboloid function in (3) as indicated in Fig. 5. To adjust the real power consumption of the smart load, the $P_{sl}$ plane (the pure-colored vertical plane) can move forward and backward along with the $P_{sl}$-axis to a required position. At the same time, to deliver the PV power, the $P_{es}$ plane (the horizontal plane with grid) can move downward from $P_{es} = 0$ to obtain a negative value of $P_{es}$. Such two planes and the paraboloid surface intercept at two points, which indicates two feasible operating points of the PV-ES system. Therefore, given a specific set of $P_{es}$ and $P_{sl}$, the proposed power-flow analysis can be used to locate a pair of feasible values of the smart-load reactive power $(Q_{sl})$.

## III. Design of PV-ES System

Based on the methodology proposed in Section II, the details on the design of the power stage, the controller, and the voltage closed loop are provided in this section.

### A. Power-Stage Design

The power-stage schematic of the proposed PV-ES system is shown in Fig. 6. The PV interfacing power converter is implemented by an active clamp flyback dc/dc converter, which is used for harvesting PV power with maximum power point tracking (MPPT) control and stepping up the PV panel voltage $(V_{pv})$ to be the dc-bus voltage $(V_{\text{bus}})$. As shown in Fig. 6, the circuit components $T_1, S_{a2}, C_1$, and $D_1$ form a conventional flyback dc/dc power converter. $C_a$ and $S_{a1}$ are added to the converter as an active clamp circuit. In addition, $D_2$ and $C_2$ are added to form a voltage multiplier circuit, which doubles the voltage conversion ratio. The input voltage $(V_{pv})$ and input current $(I_{pv})$ of this flyback converter are sensed to achieve MPPT.

The ES is realized by a conventional half-bridge dc/ac power converter, which composes $C_{b1}, C_{b2}, S_{b1}$, and $S_{b2}$. The dc bus of the ES is connected to the output of the PV interfacing power converter, while the ac port of the ES is connected between PCC and the NC load $(Z_{nc})$. $R_{b1}$ and $R_{b2}$ are added to the power stage of the ES (where $R_{b1} = R_{b2}$) to avoid capacitor voltage imbalance on $C_{b1}$ and $C_{b2}$. Real-time voltages of $V_{\text{bus}}, V_{es}$, and $V_g$ are sensed and used for the purpose of feedback control. The auxiliary dc power supply for the DSP, sensors, and driver ICs are obtained from the grid ac power, of which the details will not be discussed.

### B. Controller Design

The controller design of the PV converter and the ES is discussed in this section. Both the controllers are implemented in

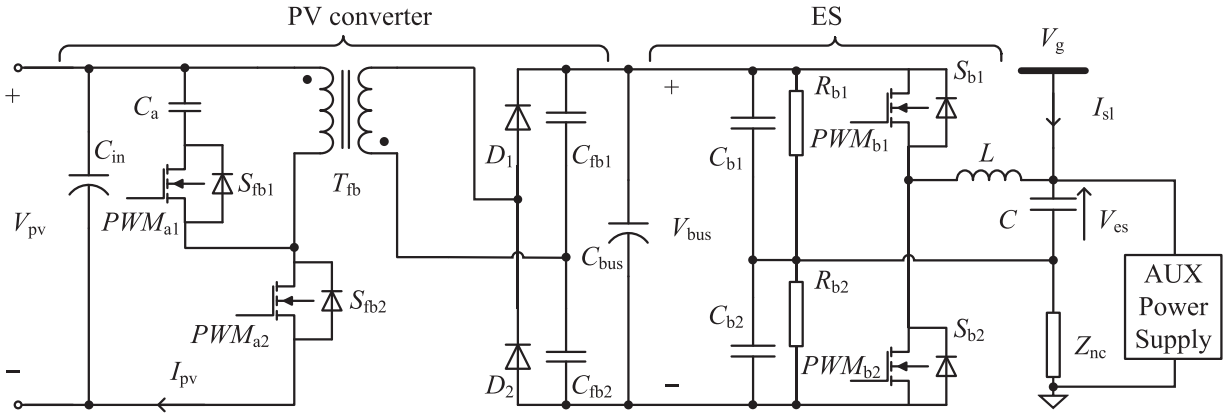


Fig. 6. Power-stage schematic of the proposed PV-ES system.

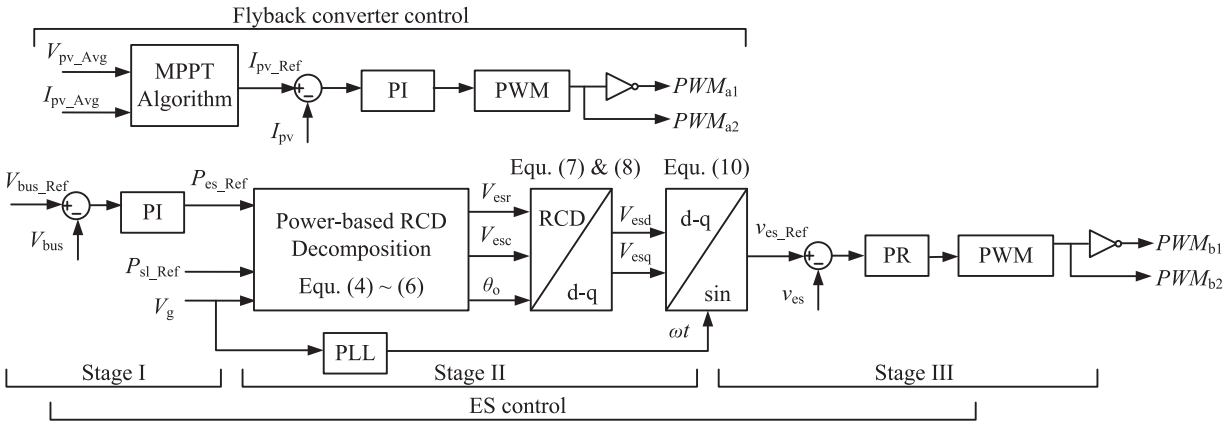


Fig. 7. Control scheme of the PV-ES system.

a single DSP controller TMS320F28069. The control block diagram of the PV-ES system is shown in Fig. 7. For the PV converter, the input current $(I_{pv})$ is regulated by a PI controller. A PV current reference $(I_{\text{pv\_Ref}})$ is obtained from the MPPT algorithm. As this paper focuses on the power management rather than the solar power harvesting method, simple PV current-voltage and power-voltage characteristics are considered (in which there is only one maximum power point on the PV power curve), and a current-based incremental conductance algorithm is adopted in this paper for the MPPT control (whose details are omitted). The output signal of the PI controller is used to generate a pair of the 20-kHz complimentary PWM signals ($PWM_{a1}$ and $PWM_{a2}$) for driving the MOSFETs $S_{a1}$ and $S_{a2}$, respectively.

The control process of the ES voltage controller comprises three stages, which are the power reference update (Stage I), the ES voltage reference calculation (Stage II), and the ES voltage regulation (Stage III).

In Stage I, the ES active power reference, $P_{\text{es\_Ref}}$, is generated by a PI controller. This PI controller is used to stabilize the dc-bus voltage by comparing the sensed $V_{\text{bus}}$ with the constant dc bus reference $(V_{\text{bus\_Ref}})$ when the PV converter is operating. Stabilizing $V_{\text{bus}}$ requires cooperation of the PV converter and ES. The fluctuation of $V_{\text{bus}}$ indicates the power imbalance between the harvested PV power and the real power ES delivered. For example, if $V_{\text{bus}}$ is higher than $V_{\text{bus\_Ref}}$, it indicates more PV power is harvested than that of ES delivered into the grid, and hence the magnitude of $P_{\text{es\_Ref}}$ increases in order to restore $V_{\text{bus}}$. Note that when the PV converter is disabled and no PV power is delivered to the output, the ES provides purely reactive power only to control $P_{sl}$. In this case, the dc voltage is not regulated to $V_{\text{bus\_Ref}}$ but allowed to vary according to the change of $V_{es}$.

In Stage II, the ES voltage reference is determined by calculating the magnitudes of $V_{esr}$, $V_{esc}$, and $\theta_o$ from the references by using (4)–(6), and then being converted into the sinusoidal form using (7)–(10).

The equations for calculation are derived from (1), and can be expressed as

$$V_{esr} = \left| V_s - \sqrt{\frac{\left(P_{\text{sl\_Ref}} - P_{\text{es\_Ref}}\right) Z_{nc}}{\cos \phi_{nc}}} \right| \tag{4}$$

$$V_{esc} = V_g \sqrt{2\left(1 - \cos \theta_o\right)} \tag{5}$$

and

$$\theta_o = \phi_{nc} \pm \arccos\left(\frac{P_{\text{sl\_Ref}} Z_{nc}}{V_g \left(V_g - V_{esr}\right)}\right). \tag{6}$$

Equation (6) indicates that there are two possible values of $\theta_{\text{o}}$ (i.e., a pair of feasible points of the system). In practice, a $\theta_{\text{o}}$ leading to less reactive power shift may be preferred, as it

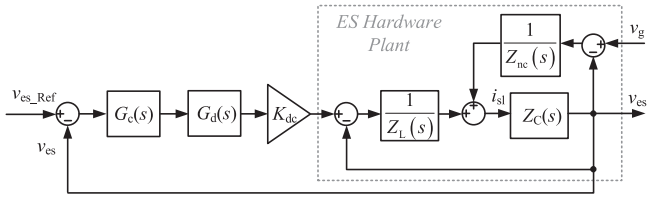


Fig. 8. Block diagram of the ES voltage control loop.

conducts less transfer of reactive power, and reduces the output voltage of ES. These benefit the dc-bus voltage control in Stage I, since the fluctuation caused by reactive power and the voltage-level requirement on components can be reduced. Choosing such a feasible operation point depends on the NC load itself. For instance, if the NC load is capacitive ($\phi_{nc} < 0$), then $\theta_o$ is the sum of the angular components as indicated in (6). In the condition where $Z_{nc}$ is purely resistive, both the choices result in the same level of reactive power shift. Therefore, $\theta_o$ can be alternatively chosen for qualitative compensation using either capacitive- or inductive-reactive power.

With the RCD voltage reference ($V_{esr}, V_{esc}$ and $\theta_o$) obtained, the ES voltage reference can be further decomposed into the *d-q* frame by using (7) and (8). Finally, the voltage reference in sinusoidal form is obtained by (10) and used for Stage III

$$V_{esd} = V_{esr}\cos\theta_o + V_{esc}\cos\left(\frac{\theta_o - \mathrm{sgn}(\theta_o)\pi}{2}\right) \tag{7}$$

and

$$V_{esq} = V_{esr}\sin\theta_o + V_{esc}\sin\left(\frac{\theta_o - \mathrm{sgn}(\theta_o)\pi}{2}\right) \tag{8}$$

where sgn(.) is defined as

$$\mathrm{sgn}(x) = \begin{cases} 1, & \text{when } x > 0 \\ -1, & \text{when } x \le 0 \end{cases} \tag{9}$$

$$v_{es\_Ref} = V_{esd}\cos(\omega t) + V_{esq}\sin(\omega t). \tag{10}$$

In Stage III, a single control loop is designed to regulate the voltage output of ES following the sinusoidal reference signal. The details of this control loop design and analysis are provided in the following section.

### C. Voltage Closed-Loop Design of ES

The block diagram of the ES voltage control loop, with reference to Figs. 6 and 7, is shown in Fig. 8, where $Z_L(s)$, $Z_C(s)$, and $Z_{nc}(s)$ stand for the dynamic impedances of the ES inductor $L_{es}$, capacitor $C_{es}$, and the NC load $Z_{nc}$, respectively. $K_{\mathrm{dc}}, G_d(s)$, and $G_c(s)$, respectively, depict the modulation gain based on dc-bus voltage, the effect of system delay causing by digital computation and PWM, and the compensator adopted in this voltage regulation. The area highlighted with a dashed line in Fig. 8 indicates the plant structure of ES and the NC load.

Based on Fig. 8, with the input of $V_g$ being recognized as an interference signal, the forward (open-loop) transfer function of this control loop can be derived as

$$G_1(s) = \frac{G_c(s)\,G_d(s)\,K_{\mathrm{dc}}Z_C(s)\,Z_{nc}(s)}{Z_L(s)\,[Z_{nc}(s) + Z_C(s)] + Z_C(s)\,Z_{nc}(s)}. \tag{11}$$

A proportional-resonant (PR) compensator $G_c$ is adopted for ES voltage control, followed by the system delay $G_d$. The transfer functions of $G_c$ and $G_d$ are designed and expressed as

$$G_c(s) = k_p + \frac{k_r \cdot 2\omega_c s}{s^2 + 2\omega_c s + {\omega_o}^2}, G_d(s) = e^{-1.5T_s s} \tag{12}$$

where $k_p, k_r, \omega_o, \omega_c$, and $T_s$ stand for the proportional parameter, resonant parameter, resonant frequency, bandwidth around the resonant frequency, and the switching period, respectively.

Hence, the closed-loop transfer functions of ES voltage control can be derived as

$$\frac{G_1(s)\cdot v_{\mathrm{es\_Ref}}(s)}{1+G_1(s)} + \frac{G_1(s)\,Z_L(s)\cdot v_g(s)}{[1+G_1(s)]\,[Z_{nc}(s)\,G_c(s)\,G_d(s)\,K_{\mathrm{dc}}]} = v_{es}(s). \tag{13}$$

Taking the parameters and specifications provided in Tables II and III in the appendix as an example, the closed-loop frequency response above 100 Hz (without compensator $G_c$) is plotted in dotted lines in Fig. 9. It indicates the system may be unstable because of the high-frequency resonance. With a PR compensator adopted in the control loop, the output only follows input reference around the resonant frequency, and greatly reduces the response to the interference in any other frequency band. The closed-loop response of the transfer function with a PR compensator is depicted by the solid lines in Fig. 9. Such frequency responses make the voltage control loop able to implement the mentioned control strategy on managing the delivered PV power.

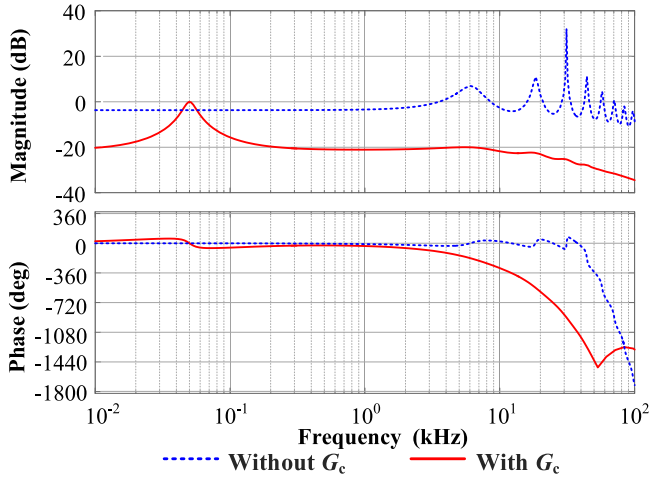


Fig. 9. Closed-loop frequency response of the ES voltage control loop.

## IV. Simulation Results and Comparisons

In this section, the proposed control methodology is first applied to a PV-ES system for a period of 24 s that is compressed from a 24-h record. Second the proposed PV-ES system is compared with the conventional PV plus BESS (PV+BESS) solution, and that of the three different existing versions of ES. The

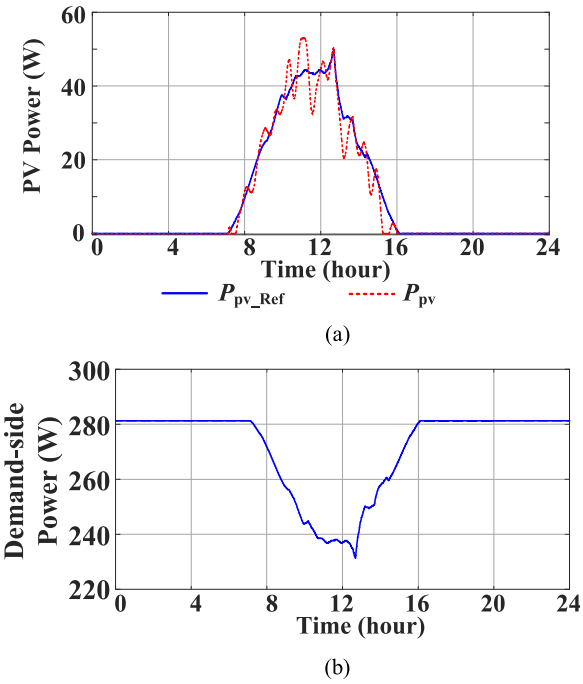


Fig. 10. Power profiles. (a) Predicted PV power ($P_{\text{pv\_Ref}}$) and the actual PV power ($P_{pv}$). (b) Predicted demand-side active power ($P_{\text{g\_Ref}}$) reference for the PV-ES system.

configuration of the simulated PV-ES system is the same as the one shown in Fig. 3.

The 24-h profiles of the predicted and actual harvested PV power ($P_{\text{pv\_Ref}}$ and $P_{pv}$) used in the simulation are plotted, as shown in Fig. 10(a). The predicted profile of this PV power is forecasted using moving average method based on the data of the solar irradiance at Hesse, Germany (latitude = 51.317°, longitude = 9.059°) on 2nd February, 2004 [41]. Though the demand-side power reference in practice can be predicted based on various information and objectives, a simple reference for demonstration is calculated by the net amount of the demand-side power as

$$P_{\text{g\_Ref}} = P_{cl} + P_{\text{nc\_nom}} - P_{\text{pv\_Ref}} \tag{14}$$

where $P_{\text{nc\_nom}}$ is a constant denoting the nominal power consumption of the NC load. To highlight the power flow control of the PV-ES with fluctuating PV power, $Z_{cl}$ and $Z_{nc}$ are simplified as constant during the simulation period. Hence, the $P_{\text{g\_Ref}}$ according to (14) is shown in Fig. 10(b). Such profiles are then compressed into a period of 24 s for simulation.

The simulation results in the first stage are shown in Fig. 11. The demand-side power is maintained at the nominal value between the periods of $t$ = 0–7 s and $t$ = 16–24 s, when the PV-ES system is deactivated due to the absence of solar energy. Fig. 11(a) shows the time-varying profile of the active power that is delivered to the power grid by the ES ($-P_{es}$). Considering the aforementioned assumption of a lossless converter, the waveform of $-P_{es}$ is exactly of the same shape as that of the actual harvest PV power in Fig. 10(a) (indicated by the dotted

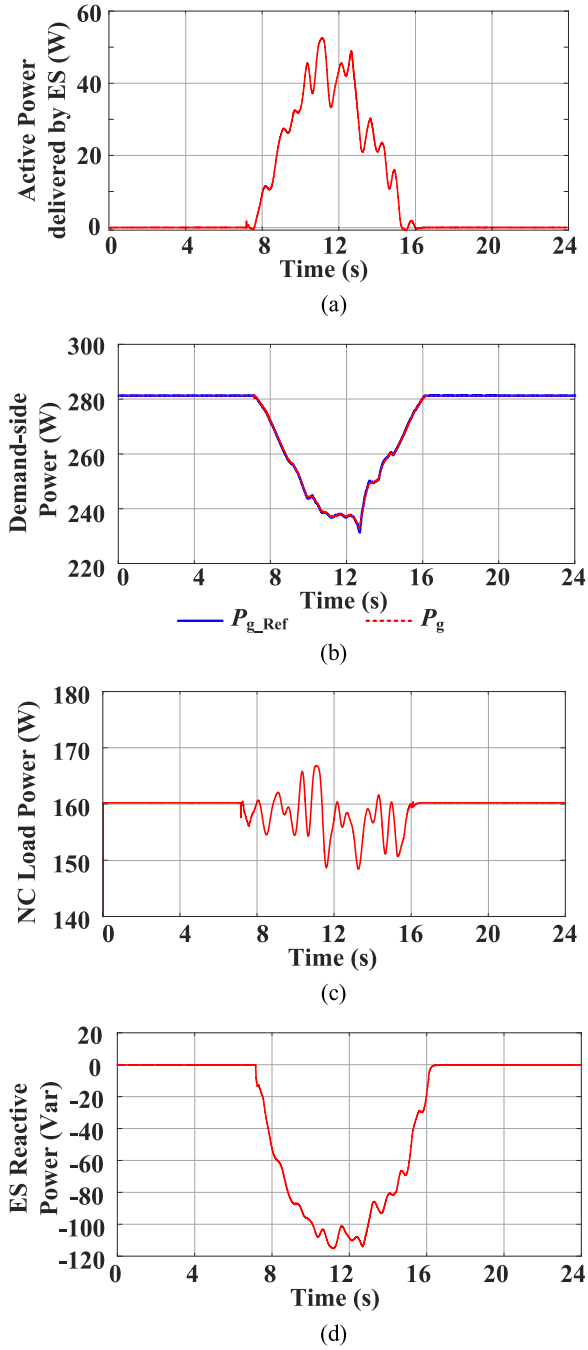


Fig. 11. Simulation results of the PV-ES system in the first stage. (a) Active power delivered by the ES ($-P_{es}$). (b) Predicted demand-side active power ($P_{\text{g\_Ref}}$) and the actual demand-side active power ($P_g$). (c) ES reactive power ($Q_{es}$). (d) NC load power ($P_{nc}$).

line), which is as expected. In Fig. 11(b), the predicted demand-side active power reference ($P_{\text{g\_Ref}}$) and the actual simulated demand-side active power ($P_g$) are plotted together for comparison. The results in Fig. 11(b) indicate that $P_g$ can be controlled by the PV-ES and it follows precisely the predicted reference.

The active power consumption of the NC load in the PV-ES configuration is plotted in Fig. 11(c) to illustrate that the

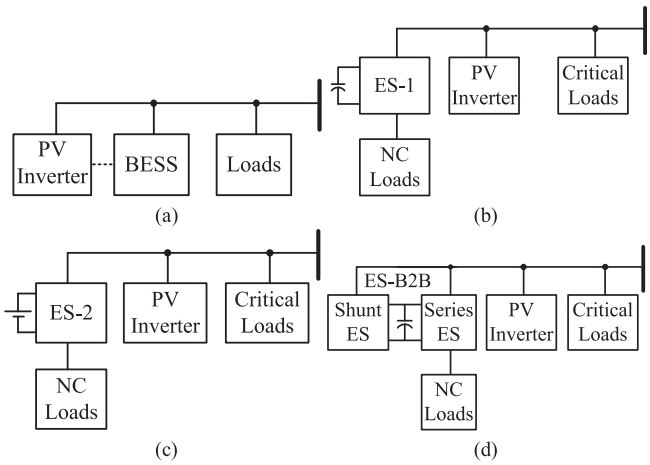


Fig. 12. Simplified diagrams of the systems for comparison. (a) PV+BESS. (b) PV+ES-1. (c) PV+ES-2. (d) PV+ES-B2B.

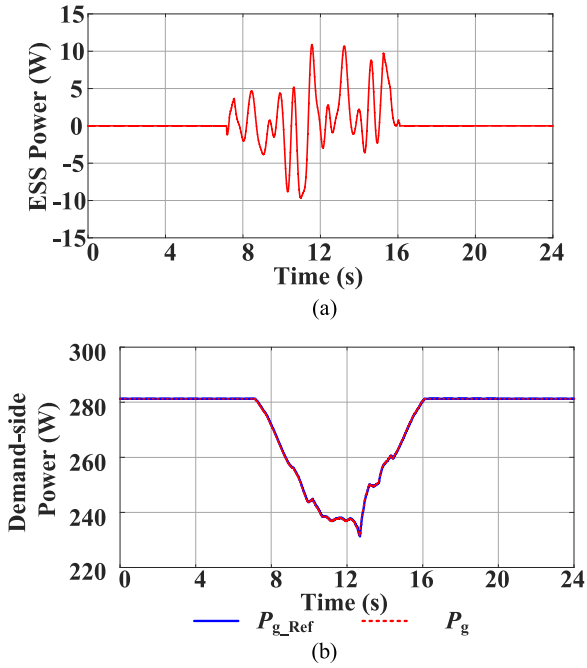


Fig. 13. Simulation results of the PV+BESS system for comparison. (a) Active power delivered by the BESS. (b) Actual demand-side active power controlled by the PV+BESS systems.

NC load is indeed operating to compensate the prediction error of the PV power. Clearly, the NC load power is adaptively adjusted closely below and above the nominal power (160 W). In addition, the reactive power transferred by the ES is plotted as shown in Fig. 11(d). The negative polarity shows that the ES reactive power is capacitive. By setting the reference of $P_{g\_Ref}$, the reactive power of ES can be made either inductive or capacitive, as can be explained using (6). Here, we arbitrarily choose the capacitive reactive power.

In the second stage, to compare with the proposed PV-ES system, the conventional ESS and three existing ES systems as solutions for fluctuation issue of PV power are tested under the same simulation configuration. Fig. 12 shows the simplified diagrams of these possible solutions.

In the conventional PV+BESS, which is capable of compensating the real power fluctuation by bi-directional power flow, is integrated with the PV inverter either via the dc bus or the PCC. The simulation results of the PV+BESS system are shown in Fig. 13. As shown in Fig. 13(a), the ESS directly compensated the error between the predicted and the actual PV power [depicted in Fig. 10(a)]. Hence, the demand-side power is controlled precisely to follow the reference, as shown in Fig. 13(b). Although the solution of PV+BESS is straightforward and effective in compensating power fluctuation, the installation of BESS is costly. The estimated average cost of BESS installation for commercial scale is $2338 USD/kW [42]. For instance, if the maximum prediction error is limited to $\pm 20\%$ of the nominal PV power, a PV system in the scale of 5 kW would require additional $2338 USD for the installation of BESS, regardless of future cost on the maintenance of batteries. In contrast, the proposed PV-ES system can save such a cost.

For comparisons, the objectives of the other three ES systems are set the same as the PV-ES system as a power balancer. Moreover, ES-2 and ES-B2B are preset to regulate the power factor of the smart loads at 0.9. This is a unique function of ES-2 and ES-B2B, which is in contrast to the proposed PV-ES system, since they can be configured to control the active and reactive power consumption simultaneously. Fig. 14 shows the simulation results of three ES systems during the period. As observed from Fig. 14(a), the active power delivered by ES-1 is almost zero as it can only provide reactive compensation. Fig. 14(b) shows the demand-side active power consumption under the regulation of the ES systems. The profiles of ES-2 and ES-B2B illustrate that both these ES are capable of tracking the reference as well as the PV-ES. However, the profile of ES-1 contains obvious deviations, which is attributed to the limitation of ES-1. The reason is, with a purely resistive NC load, by providing reactive power, the ES-1 can only decrease (but not increase) the active power consumption of the smart load from the nominal value. Therefore, when the actual PV power is more than the predicted value, the smart load associated with ES-1 cannot consume additional power to compensate the deviation. This is also confirmed by the corresponding NC load consumption and ES reactive power as indicated in Fig. 14(c) and (d), respectively. As a result, ES-1 cannot achieve the same objective of the proposed PV-ES.

Although ES-2 can provide 1) precise active power consumption control of the smart load as well as the PV-ES and 2) controllable reactive power compensation which is better than the PV-ES, the operation requires real power from its battery storage. As shown in Fig. 14(a), ES-2 requires around 38 W for this 160-W NC load and the maximum-50-W PV generation. Additionally, as shown in Fig. 14(c), the operation of smart load associated with ES-2 sacrifices the NC load severely. Here, the power of NC load is 198 W at the static state (for power factor regulation) and reaches 224 W during the dynamic state (for both the active power and power factor regulation). In

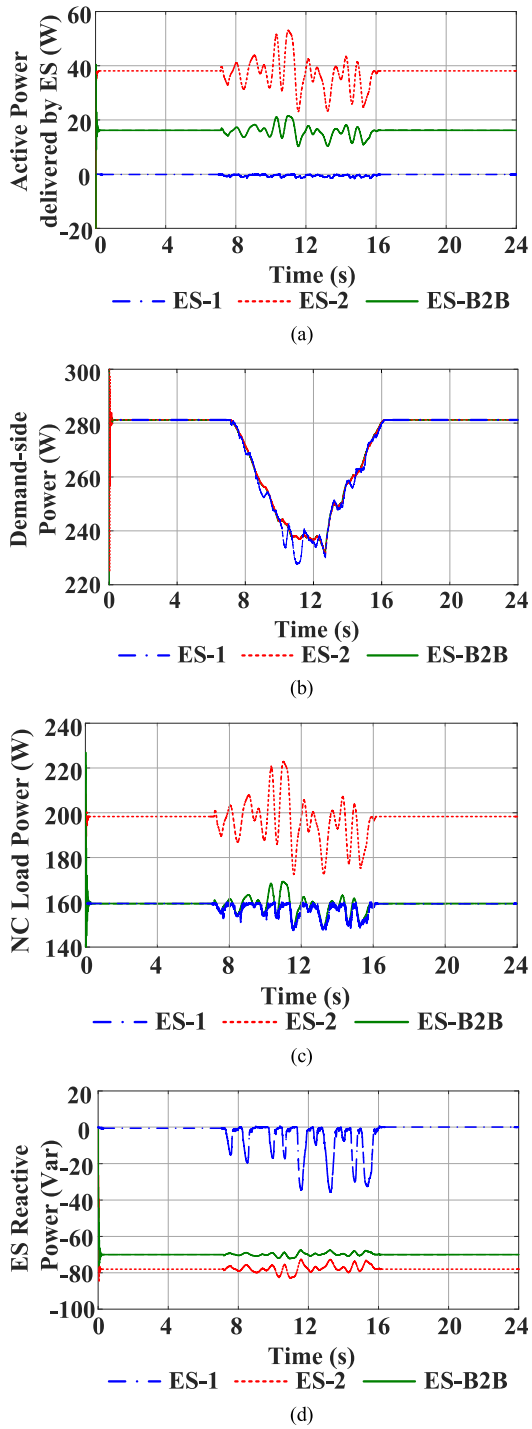


Fig. 14. Simulation results of the three types of ES systems (ES-1, ES-2, and ES-B2B) for comparison. (a) Active power delivered by the ES systems. (b) Actual demand-side active power controlled by the ES systems. (c) Reactive power consumed by the ES systems. (d) NC load power in the ES systems.

conclusion, while ES-2 can achieve the same objective as that of the proposed PV-ES, this comes at the expense of a higher cost and poorer performance of the NC load.

By contrast, ES-B2B performs the best among the three ES systems in the study. With the same precise active power control

TABLE I
SUMMARY OF THE RESULTS OF DIFFERENT COMPARATIVE SOLUTIONS

| | Energy storage requirement | Demand-side active power control | Demand-side reactive power control | NC Load power variation | Implemental cost |
|---|---|---|---|---|---|
| PV-ES | *N/A* | *Good* | *Limited* | *Slight* | *Low* |
| PV+ESS | *High* | *Good* | *Good* | *N/A* | *High* |
| PV+ES-1 | *N/A* | *Limited* | *Limited* | *Slight* | *Medium* |
| PV+ES-2 | *High* | *Good* | *Good* | *Severe* | *High* |
| PV+ES-B2B | *N/A* | *Good* | *Good* | *Slight* | *Medium* |

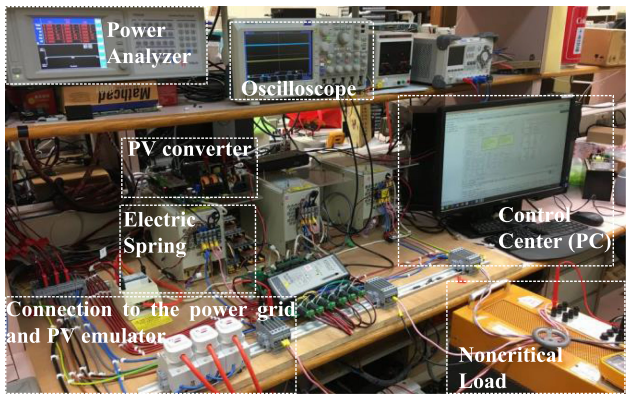


Fig. 15. Hardware platform setup of a PV-ES system.

of the smart load, the power delivered by the series part of ES-B2B, which is shown in Fig. 14(a), comes from the grid itself via the shunt ES. According to Yan *et al.* [38], the power flow of ES-B2B in operation possesses a broader range and higher effectiveness in regulating the power consumption than that of ES-2. As depicted in Fig. 14(a) and (d), the active/reactive power through ES-B2B is smaller than that of ES-2. Also, the power fluctuation of NC load is controlled at the same level as that of PV-ES. In other words, ES-B2B performs as well as the proposed PV-ES as a power balancer. However, the implementation cost of ES-B2B is much higher than that of PV-ES. While the proposed PV-ES provides a compact configuration including both the PV converter and the ES inverter, the ES-B2B system requires a back-to-back converter (combined with a shunt and a series ES converters), an isolation transformer, and an individual PV inverter. Table I summarizes the comparisons in the second stage.

To summarize, in terms of stabilizing the demand-side power that is influenced by the fluctuating PV power, the proposed PV-ES system performs as well as, if not better than, the other options currently available. However, the low implementation cost of its converter circuit and its battery-free configuration makes it much more competitive as a practical solution. If deployed in a power system with existing ESS, diesel generators and load control strategies, the PV-ES will further benefit the system: 1) PV-ES will be compatible with common load control strategies as it provides continuous power flow adjustment as a smart load; and 2) PV-ES may help to reduce the requirement

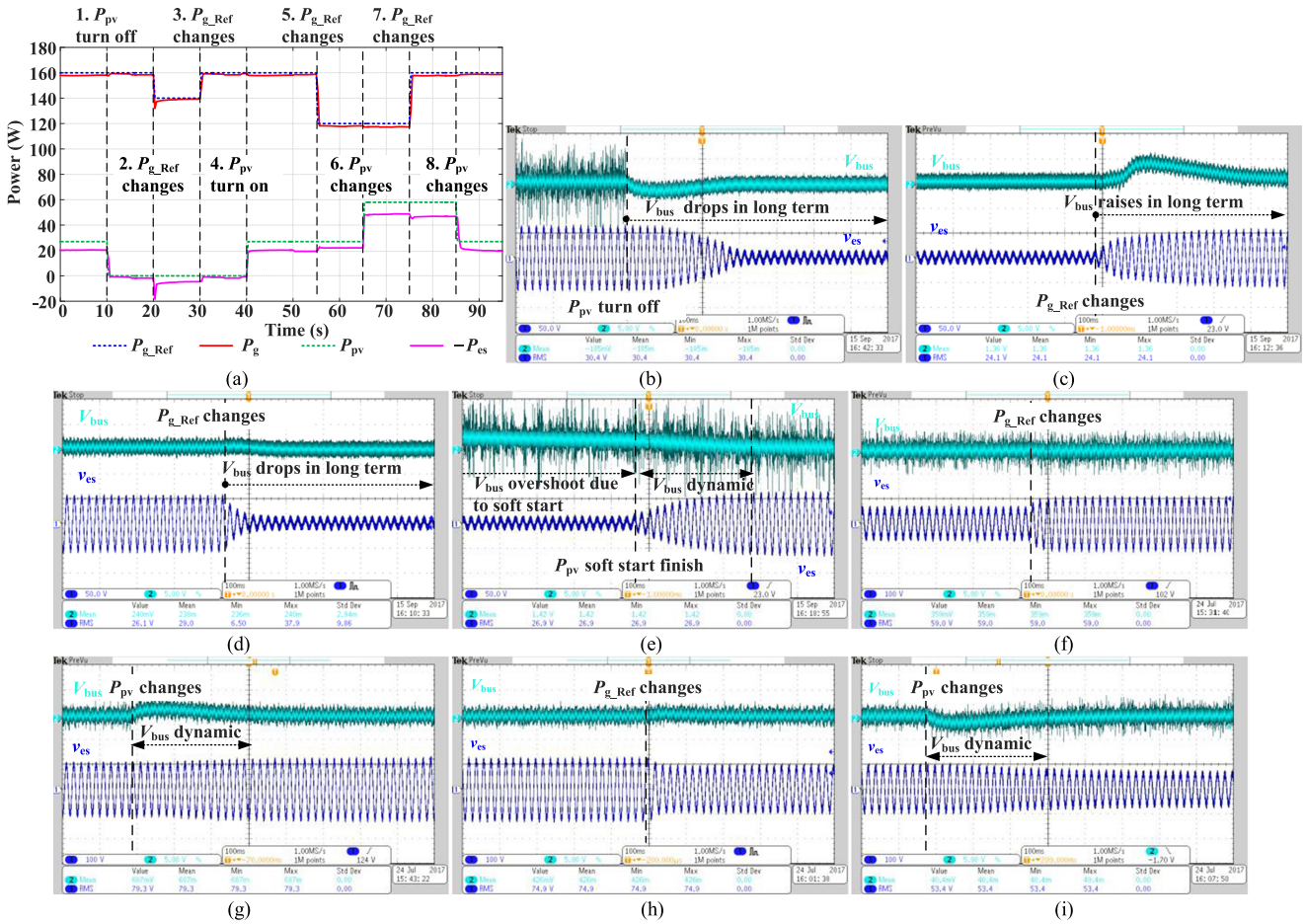


Fig. 16. Measured dynamic responses of PV-ES system against power references step-change. (a) Measured dynamic power information over the full experiment period. (b) First step-change waveform. (c) Second step-change waveform. (d) Third step-change waveform. (e) Fourth step-change waveform. (f) Fifth step-change waveform. (g) Sixth step-change waveform. (h) Seventh step-change waveform. (i) Eighth step-change waveform.

of the rating power of ESS and diesel generators, as it mitigates the power fluctuation of PV power.

## V. Experimental Results

A laboratory-scale power system is set up to verify the feasibility of the proposed PV-ES system and the control methodology. The configuration of this experiment is similar to the electrical diagram shown in Fig. 3, except that $Z_{cl}$ is ignored temporarily (as it only consumes constant power in the experimental case with stable grid voltage). Therefore, the demand-side power is equal to the smart load power ($P_g = P_{sl}$). $Z_{nc}$ is represented by a resistive load with a value of 75.5 Ω. The specifications of the PV-ES power stage is shown in Table III. A universal power analyzer PM6000 and an oscilloscope DPO3034 are used for electrical data measurement. The actual hardware setup is shown in Fig. 15.

The experiment is divided into two stages. The objective of the first stage is to test the dynamic performance of the PV-ES system on its power flow control ability in different conditions, including switch-ON/OFF of the PV power and step-changed power references. In this stage, the PV panel array is represented by a programmable dc source DP802. Since the MPPT algorithm is not activated at this stage, $V_{pv}$ is set constant at 30 V. $I_{pv}$ is adjusted to emulate a specific amount of the actual harvested PV power. The experimental results are shown in Fig. 16. The active power reference of the demand side $P_{\text{g\_Ref}}$, the correspondingly active power of the demand side $P_g$, the harvested PV power $P_{pv}$, and the actual delivered power of PV-ES $-P_{es}$, are shown in Fig. 16(a). The transient waveforms of each step-change are provided from Fig. 16(b)–(i), in which $V_{\text{bus}}$ (upper profile) and $V_{es}$ (lower profile) are indicated.

At the beginning of stage one, $V_{\text{bus}}$ is regulated to 280 V, and $P_{\text{g\_Ref}}$ is set at 160 W (the nominal power) whilst 27 W of $P_{pv}$ is harvested by the PV-ES system. To verify the ability of PV-ES with PV power switch-OFF, $P_{pv}$ is step-changed to zero at $t = 10$ s. It is observed from Fig. 16(b) that the switch-OFF of the solar power causes an instant voltage drop of the dc bus, and $V_{es}$ are cut correspondingly to restore the $V_{\text{bus}}$. In this condition, as no energy is pumped from the PV converter, $V_{\text{bus}}$ will keep decreasing, regardless of the voltage regulation, until it reaches a self-balance with $V_{es}$ (which ideally should be providing purely reactive power). Then, $P_{\text{g\_Ref}}$ is step-changed at $t = 20$ s and $t = 30$ s, to verify the ability of PV-ES to regulate the power

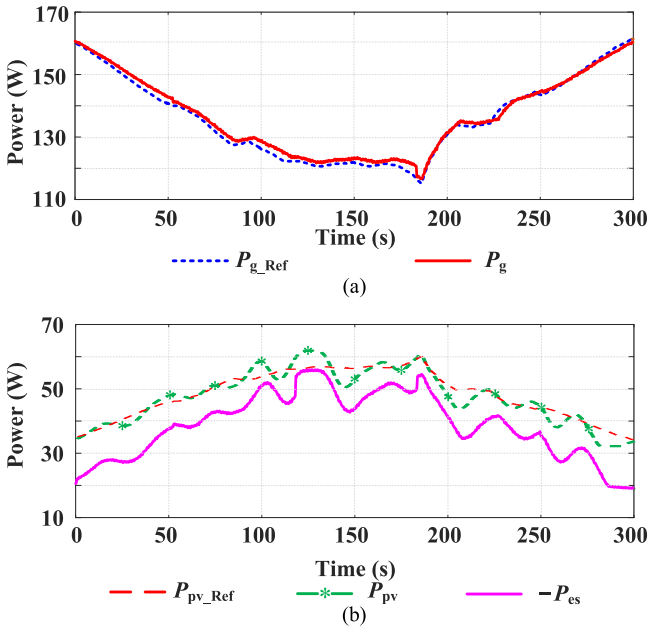


Fig. 17. Measured power information of the PV-ES with predicted references. (a) Predicted demand-side active power $(P_{g\_Ref})$ and the actual demand-side active power $(P_g)$. (b) Predicted reference of PV power $(P_{pv\_Ref})$, the actual harvested PV power $(P_{pv})$, and the active power delivered by the ES $(-P_{es})$.

consumption of the smart load without PV power. The responses in Fig. 16(a) indicate that the PV-ES can still regulate the active power of the smart load by using reactive power (similar to the ES-1). Note that the ES absorbs a small amount of the energy when $P_{g\_Ref} = 140$ W, as the rise of $V_{es}$ [Fig. 16(c) and (d)] leads to the increase of $V_{bus}$ and inverter power loss. At $t =$ 40 s, the PV converter is enabled again, and the PV-ES turns the flyback converter on with soft start (using constant duty-cycle to pump the $V_{bus}$). When an overshoot of the $V_{bus}$ is detected, the controller is restarted to regulate $V_{bus}$, as shown in Fig. 16(e).

After the PV-ES system comes back to its initial condition, for the sake of verifying the performance of the PV-ES with PV power switch-ON, $P_{g\_Ref}$ and $P_{pv}$ are individually step-changed at $t = 55$ s, $t = 65$ s, $t = 75$ s, and $t = 85$ s. It can be observed from Fig. 16(a) that while the waveform of $P_g$ follows accurately the power reference $P_{g\_Ref}$, the waveform of $-P_{es}$ follows the reference $P_{pv}$ in its shape but with significant deviation. This is due to the power loss of the converter power. For each step-change, the instantaneous responses of $V_{es}$ and $V_{bus}$ are provided in Fig. 16(f)–(i). In the fifth and seventh step-change, there are only changes in $P_{g\_Ref}$ but no PV power fluctuation involved. As a result, $V_{es}$ can be regulated within three ac cycles, as shown in Fig. 16(f) and (h). In the sixth and eighth step-change, changes in $P_{pv}$ cause firstly a fluctuation in $V_{bus}$, of which led to the PI controller making an adjustment to restore $V_{bus}$. As a result, the regulation of $V_{es}$ appears to require a longer settling time (around 18 ac cycles) than the aforementioned two cases. Considering that the PV power fluctuation in practice is slow (bandwidth $<1$ Hz), such a dynamic response of the PV-ES system is relatively fast in comparison.

In the second stage, the proposed system is configured to harvest the solar power and to control the power of the smart load with the predicted profiles adopted in the simulation. The references and experimental measurements are depicted in Fig. 17. The solar power is provided by a PV emulator AMETEK-ETS80X10.5C with preloaded profile and harvested by the PV converter in MPPT. The actual harvested PV power $(P_{pv})$ is plotted as a dotted line with stars, which is deliberately distorted from the predicted reference $(P_{pv\_Ref})$ based on the aforementioned irradiation data. Meanwhile, the waveform of the predicted active power on demand side $(P_{g\_Ref})$, which is acquired by (14) and plotted as a dotted line, is preloaded in the PV-ES as the reference. As shown in Fig. 17(a) with a solid line, the measured active power on demand side $(P_g)$ follows the dynamic reference very well. The power delivered by the PV-ES $(-P_{es})$, as shown in Fig. 17(b) with a solid line, has the same shape as that of $P_{pv}$, but with amplitude deviation due to power loss.

## VI. Conclusion

In this paper, a PV-ES system that is acting as a power balancer, is adopted in power distribution networks that have a high penetration of PV power generation, to assist in grid stabilization. The power flow analysis and implementation design in single-phase power system ensure that the proposed PV-ES can harvest the fluctuating MPPT PV power without involving battery storage, and adaptively control the active power consumption of the ES-associated smart load simultaneously. A comparison of the proposed PV-ES solution with the conventional BESS solution and those based on previous types of ES, validates that the former is a relatively better solution with a lower installation cost. As indicated by the simulation and experimental results, the issue of a power imbalance that may be resulting from a PV power prediction error, can be alleviated. It has also been illustrated that satisfactory dynamic behavior of the system via demand-side management based on the ES-associated smart load can be achieved.

## Appendix

TABLE II
Parameters of the Controllers

| Symbol | Description | Value |
|---|---|---|
| $k_p$ | PR controller proportional parameter (ES) | 0.05 |
| $k_r$ | PR controller resonant parameter (ES) | 384 |
| $\omega_o$ | PR controller resonant frequency (ES) | $100\pi$ |
| $\omega_c$ | PR controller bandwidth (ES) | 0.05 |
| $k_{pdc}$ | PI proportional parameter (DC bus) | 0.03 |
| $k_{idc}$ | PI integral parameter (DC bus) | 0.01 |
| $k_{pfb}$ | PI proportional parameter (Flyback) | 0.06 |
| $k_{ifb}$ | PI integral parameter (Flyback) | 200 |

TABLE III
SPECIFICATIONS OF THE POWER STAGE

| Symbol | Description | Value |
|---|---|---|
| $C_{in}$ | Flyback input capacitor | AVX, FFB44E0476K, Film, 47μF, 100 V (2 pcs) |
| $S_{a1}$, $S_{a2}$ | Flyback MOSFETs | IR, IRFB4227PBF, 65 A, 200 V |
| $T_1$ | Flyback transformer | VITEC, 58PR6962 |
| $C_a$ | Flyback clamping capacitor | TDK, C3225X7S2A475M, MLCC, 4.7 μF, 100 V (2pcs) |
| $D_1$, $D_2$ | Flyback output diodes | Cree, CSD10060G, Schottky, 10 A, 600 V |
| $C_1$, $C_2$ | Flyback output capacitors | TDK, B32674D4155K, 1.5μF, 450 V |
| $C_{bus}$ | DC bus capacitor | Nippon Chemi-con, EKXG451E101MM40S, 100 μF, 450 V |
| $C_{b1}$, $C_{b2}$ | ES capacitors | Nippon Chemi-con, ELXQ251VSN152MA50S, 1500 μF, 250 V |
| $R_{b1}$, $R_{b2}$ | DC bus balance resistors | Arcol, HS25, 25 W, 25 kΩ |
| $S_{b1}$, $S_{b2}$ | ES MOSFETs | IR, IRFP31N50L, 31A, 500 V |
| $L_{es}$ | ES output inductor | AMCC, 500 mH, 16A |
| $C_{es}$ | ES output capacitor | HJC, MKP-2250305AB27U, 2.2μF, 310 V (3 pcs) |
| $f_{fb}$ | Flyback switching frequency | 20 kHz |
| $f_{es}$ | ES switching frequency | 20 kHz |

## REFERENCES


[1] T. Kerekes, R. Teodorescu, M. Liserre, C. Klumpner, and M. Sumner, "Evaluation of three-phase transformerless photovoltaic inverter topologies," *IEEE Trans. Power Electron.*, vol. 24, no. 9, pp. 2202–2211, Sep. 2009.

[2] Y. Karimi, H. Oraee, M. S. Golsorkhi, and J. M. Guerrero, "Decentralized method for load sharing and power management in a PV/battery hybrid source islanded microgrid," *IEEE Trans. Power Electron.*, vol. 32, no. 5, pp. 3525–3535, 2017.

[3] F. Blaabjerg, Z. Chen, and S. B. Kjaer, "Power electronics as efficient interface in dispersed power generation systems," *IEEE Trans. Power Electron.*, vol. 19, no. 5, pp. 1184–1194, Sep. 2004.

[4] F. Blaabjerg, Y. Yang, D. Yang, and X. Wang, "Distributed power-generation systems and protection," *Proc. IEEE*, vol. 105, no. 7, pp. 1311–1331, Jul. 2017.

[5] W. Kempton and J. Tomic, "Vehicle-to-grid power implementation: From stabilizing the grid to supporting large-scale renewable energy," *J. Power Sources*, vol. 144, no. 1, pp. 280–294, Jun. 2005.

[6] X. Wang and Q. Liang, "Energy management strategy for plug-in hybrid electric vehicles via bidirectional vehicle-to-grid," *IEEE Syst. J.*, vol. 11, no. 3, pp. 1789–1798, Sep. 2017.

[7] C. Wang *et al.*, "A highly integrated and reconfigurable microgrid testbed with hybrid distributed energy sources," *IEEE Trans. Smart Grid*, vol. 7, no. 1, pp. 451–459, Jan. 2016.

[8] Y. Han, H. Li, P. Shen, E. A. A. Coelho, and J. M. Guerrero, "Review of active and reactive power sharing strategies in hierarchical controlled microgrids," *IEEE Trans. Power Electron.*, vol. 32, no. 3, pp. 2427–2451, 2017.

[9] S. B. Kjaer, J. K. Pedersen, and F. Blaabjerg, "A review of single-phase grid-connected inverters for photovoltaic modules," *IEEE Trans. Ind. Appl.*, vol. 41, no. 5, pp. 1292–1306, Sep. 2005.

[10] F. Olivier, P. Aristidou, D. Ernst, and T. Van Cutsem, "Active management of low-voltage networks for mitigating overvoltages due to photovoltaic units," *IEEE Trans. Smart Grid*, vol. 7, no. 2, pp. 926–936, 2016.

[11] C. Whitaker, J. Newmiller, M. Ropp, and B. Norris, "Renewable systems interconnection study: distributed photovoltaic systems desig and technology requirements," *Sandia National Laboratories*, Albuquerque, NM, USA and Livermore, CA, USA, Tech. Rep. SAND2008-0946 P, 2008.

[12] Y. Yang, H. Li, A. Aichhorn, J. Zheng, and M. Greenleaf, "Sizing strategy of distributed battery storage system with high penetration of photovoltaic for voltage regulation and peak load shaving," *IEEE Trans. Smart Grid*, vol. 5, no. 2, pp. 982–991, Mar. 2014.

[13] REN21 Secretariat, "Renewables 2017: Global status report," 2017 REN21. [Online]. Available: http://www.ren21.net/wp-content/uploads/2017/06/17-8399_GSR_2017_Full_Report_0621_Opt.pdf

[14] R. Margolis, D. Feldman, and D. Boff, "Q4 2016/Q1 2017 Solar Industry Update. Sunshot, U.S. Department of Energy," Apr. 2017. [Online]. Available: https://www.nrel.gov/docs/fy17osti/68425.pdf

[15] Renewables 2017: Analysis and Forecasts to 2022 Executive Summary. "International energy agency," Oct. 2017. [Online]. Available: https://www.iea.org/Textbase/npsum/renew2017MRSsum.pdf

[16] J. D. Glover, M. S. Sarma, and T. Overbye, *Power System Analysis and Design*. 5th ed. Stamford, CT, USA: Cengage Learning, Jan. 2011.

[17] C. L. Masters, "Voltage rise: the big issue when connecting embedded generation to long 11 kV overhead lines," *Power Eng. J.*, vol. 16, no. 1, pp. 5–12, Feb. 2002.

[18] R. A. Walling, R. Saint, R. C. Dugan, J. Burke, and L. A. Kojovic, "Summary of distributed resources impact on power delivery systems," *IEEE Trans. Power Del.*, vol. 23, no. 3, pp. 1636–1644, Jul. 2008.

[19] Q. Fu *et al.*, "Microgrid generation capacity design with renewables and energy storage addressing power quality and surety," *IEEE Trans. Smart Grid*, vol. 3, no. 4, pp. 2019–2027, Dec. 2012.

[20] X. Liu, A. Aichhorn, L. Liu, and H. Li, "Coordinated control of distributed energy storage system with tap changer transformers for voltage rise mitigation under high photovoltaic penetration," *IEEE Trans. Smart Grid*, vol. 3, no. 2, pp. 897–906, Jun. 2012.

[21] T. T. Hashim, A. Mohamed, and H. Shareef, "A review on voltage control methods for active distribution networks," *Prz. Elektrotech*, vol. 88, pp. 304–312, 2012.

[22] T. Stetz, F. Marten, and M. Braun, "Improved low voltage grid-integration of photovoltaic systems in Germany," *IEEE Trans. Sustain. Energy*, vol. 4, no. 2, pp. 534–542, Apr. 2013.

[23] R. Tonkoski, L. A. C. Lopes, and T. H. M. El-Fouly, "Coordinated active power curtailment of grid connected PV inverters for overvoltage prevention," *IEEE Trans. Sustain. Energy*, vol. 2, no. 2, pp. 139–147, Apr. 2011.

[24] S. Alyami, Y. Wang, C. Wang, J. Zhao, and B. Zhao, "Adaptive real power capping method for fair overvoltage regulation of distribution networks with high penetration of pv systems," *IEEE Trans. Smart Grid*, vol. 5, no. 6, pp. 2729–2738, Nov. 2014.

[25] M. Zillmann, R. Yan, and T. K. Saha, "Regulation of distribution network voltage using dispersed battery storage systems: a case study of a rural network," in *Proc. IEEE Power Energy Soc. General Meeting*, Jul. 2011, pp. 1–8.

[26] K. H. Chua, Y. S. Lim, P. Taylor, S. Morris, and J. Wong, "Energy storage system for mitigating voltage unbalance on low-voltage networks with photovoltaic systems," *IEEE Trans. Power Del.*, vol. 27, no. 4, pp. 1783–1790, Oct. 2012.

[27] W. A. Omran, M. Kazerani, and M. M. A. Salama, "Investigation of methods for reduction of power fluctuations generated from large grid-connected photovoltaic systems," *IEEE Trans. Energy Convers.*, vol. 26, no. 1, pp. 318–327, Mar. 2011.

[28] O. Zehner, "Unclean at any speed," *IEEE Spectrum*, vol. 50, no. 7, pp. 40–45, Jul. 2013.

[29] S. Hashemi, J. Ostergaard, and G. Yang, "A scenario-based approach for energy storage capacity determination in LV grids with high PV penetration," *IEEE Trans. Smart Grid*, vol. 5, no. 3, pp. 1514–1522, May 2014.

[30] E. Yao, P. Samadi, V. W. S. Wong, and R. Schober, "Residential demand side management under high penetration of rooftop photovoltaic units," *IEEE Trans. Smart Grid*, vol. 7, no. 3, pp. 1597–1608, May 2016.

[31] P. Samadi, H. Mohsenian-Rad, V. W. S. Wong, and R. Schober, "Real-time pricing for demand response based on stochastic approximation," *IEEE Trans. Smart Grid*, vol. 5, no. 2, pp. 789–798, Mar. 2014.

[32] G. Strbac, "Demand side management: benefits and challenges," *Energy Policy*, vol. 36, no. 12, pp. 4419–4426, Dec. 2008.

[33] M. Slezak and K. Murphy, "NSW could face power shortages as temperature rises on energy policy," *The Guardian*, Feb. 2017. [Online]. Available: https://www.theguardian.com/australia-news/2017/feb/09/nsw-power-shortage-warning-after-revelation-sa-blackouts-forecast-hours-beforehand/

[34] S. Y. R. Hui, C. K. Lee, and F. F. Wu, "Electric springs – a new smart grid technology," *IEEE Trans. Smart Grid*, vol. 3, no. 3, pp. 1552–1561, Sep. 2012.

[35] P. Kanjiya and V. Khadkikar, "Enhancing power quality and stability of future smart grid with intermittent renewable energy sources using electric springs," in *Proc. IEEE Renew. Energy Res. Appl.*, Oct. 2013, pp. 918–922.

[36] K. L. Cheng, X. Luo, and C. K. Lee, "Reactive power flow control of grid tie inverter to enhance the stability of power grid," in *Proc. IEEE Int. Symp. Power Electron. Distrib. Gener. Syst.*, 2014, pp. 1–8.

[37] S. C. Tan, C. K. Lee, and S. Y. Hui, "General steady-state analysis and control principle of electric springs with active and reactive power compensations," *IEEE Trans. Power Electron.*, vol. 28, no. 8, pp. 3958–3969, Aug. 2013.
[38] S. Yan *et al.*, "Extending the operating range of electric spring using back-to-back converter: hardware implementation and control," *IEEE Trans. Power Electron.*, vol. 32, no. 7, pp. 5171–5179, Jul. 2017.
[39] J. Shi, W. J. Lee, Y. Liu, Y. Yang, and P. Wang, "Forecasting power output of photovoltaic systems based on weather classification and support vector machines," *IEEE Trans. Ind. Appl.*, vol. 48, no. 3, pp. 1064–1069, May 2012.
[40] K. T. Mok, S. C. Tan, and S. Y. Hui, "Decoupled power angle and voltage control of electric springs," *IEEE Trans Power Electron.*, vol. 31, no. 2, pp. 1216–1229, Feb. 2016.
[41] Time series of solar radiation data in Germany on 2nd Feb. 2004 (Date last accessed 7-Aug-2017). The SoDa Service, 2014. [Online]. Available: http://www.soda-is.com/
[42] J. McLaren, P. Gagnon, K. Anderson, E. Elgqvist, R. Fu, and T. Remo, "Battery energy storage market: commercial scale, lithium-ion projects in the U.S.," National Renewable Energy Laboratory, Golden, CO, USA, Oct. 2016.

**Tianbo Yang** (S'15) received the B.Eng. and M.Phil. degrees in automation and control engineering from the Harbin Institute of Technology, China, in 2012 and 2014, respectively. He is currently working toward the Ph.D. degree at the Department of Electrical and Electronic Engineering, the University of Hong Kong.

His research interests include power electronic technologies in smart grid and energy storage system.

**Kwan-Tat Mok** (S'14) received the B.Eng. (Hons.) and M.Phil. degrees in electronic and information engineering from the Hong Kong Polytechnic University, in 2009 and 2012, respectively, and the Ph.D. degree in electrical and electronic engineering from the University of Hong Kong, Hong Kong, in 2016.

He is currently a Senior Engineer at NISI Group, Hong Kong, working on the research and development of noninvasive surgical medical devices. In 2007, he worked as an Engineering Trainee in Solomon Systech Limited, Hong Kong, for a one-year internship program. From September 2011 to February 2013, he was an Embedded System Engineer in Cwlinux Limited, Hong Kong. From July to August 2015, he was a Visiting Postgraduate Student in Department of Electrical and Electronic Engineering, Imperial College London. His research interests include smart grid technologies, power converters for light-emitting diodes, and surgical robotics.

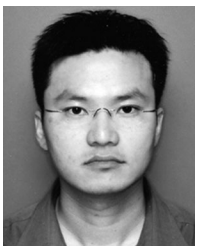

**Siu-Shing Ho** received the B.Eng. (Hons.) degree in electronic engineering from the City University of Hong Kong, Kowloon Tong, Hong Kong, in 2008.

From 1996 to 2006, he was an Electronic Engineer in the Astec Custom Power (HK) LTD. He is currently a Research Associate in Power Electronics Research Group, University of Hong Kong, Hong Kong. His research interests include control of power electronics and smart grid.

**Siew-Chong Tan** (M'06–SM'11) received the B.Eng. (Hons.) and M.Eng. degrees in electrical and computer engineering from the National University of Singapore, Singapore, in 2000 and 2002, respectively, and the Ph.D. degree in electronic and information engineering from the Hong Kong Polytechnic University, Hong Kong, in 2005.

From October 2005 to May 2012, he worked as a Research Associate, Postdoctoral Fellow, Lecturer, and an Assistant Professor in the Department of Electronic and Information Engineering, Hong Kong Polytechnic University, Hong Kong. From January to October 2011, he was a Senior Scientist in Agency for Science, Technology and Research (A*Star), Singapore. He is currently a Professor in Department of Electrical and Electronic Engineering, The University of Hong Kong, Hong Kong. He was a Visiting Scholar at Grainger Center for Electric Machinery and Electromechanics, University of Illinois at Urbana-Champaign, Champaign, from September to October 2009, and an Invited Academic Visitor of Huazhong University of Science and Technology, Wuhan, China, in December 2011. His research interests are focused in the areas of power electronics and control, LED lightings, smart grids, and clean energy technologies. He is a coauthor of the book *Sliding Mode Control of Switching Power Converters: Techniques and Implementation* (Boca Raton: CRC, 2011).

Prof. Tan serves extensively as a Reviewer for various IEEE/IET transactions and journals on power, electronics, circuits, and control engineering. He is an Associate Editor for the IEEE TRANSACTIONS ON POWER ELECTRONICS.

**Chi-Kwan Lee** (M'08–SM'14) received the B.Eng. and Ph.D. degrees in electronic engineering from the City University of Hong Kong, Kowloon, Hong Kong, in 1999 and 2004, respectively.

He is currently an Associate Professor at the Department of Electrical and Electronic Engineering, The University of Hong Kong. Since 2010, he has been a Visiting Researcher with Imperial College London. He was a Postdoctoral Research Fellow in the Power and Energy Research Centre at the National University of Ireland, Galway, from 2004 to 2005. In 2006, he joined the Centre of Power Electronics in City University of Hong Kong as a Research Fellow. In 2008–2011, he was a Lecturer of electrical engineering at the Hong Kong Polytechnic University. He is a coinventor of the Electric Springs and planar EMI filter. His current research interests include wireless power transfer, clean energy technologies, and smart grids.

Dr. Lee received the IEEE Power Electronics Transactions First Prize Paper Award for his publications on Mid-Range Wireless Power Transfer in 2015.

**Ron S. Y. Hui** (M'87–SM'94–F'03) received the B.Sc. (Eng. Hons.) degree in electrical and electronic engineering from the University of Birmingham, Birmingham, U.K., in 1984, and the D.I.C. and Ph.D. degrees in electrical engineering from Imperial College London, London, U.K., in 1987.

He currently holds the Philip Wong Wilson Wong Chair Professorship at The University of Hong Kong and a part-time Chair Professorship at Imperial College London. He has published more than 400 technical papers, including more than 250 refereed journal publications and book chapters. More than 60 of his patents have been adopted by industry. His inventions on wireless charging platform technology underpin key dimensions of Qi, the world's first wireless power standard, with freedom of positioning, and localized charging features for wireless charging of consumer electronics. He developed the Photo-Electro-Thermal Theory for LED systems.

Dr. Hui received the 2010 IEEE Rudolf Chope R&D Award from the IEEE Industrial Electronics Society, the 2010 IET Achievement Medal (The Crompton Medal), and the 2015 IEEE Technical Field Award (IEEE William E. Newell Power Electronics Award). He is a Fellow of the Australian Academy of Technological Sciences and Engineering, and also the Royal Academy of Engineering, U.K.